Automatic model order reduction for systems with frequency-dependent material properties

Quirin Aumann[a,*], Elke Deckers[b,e], Stijn Jonckheere[c,d], Wim Desmet[c,e], Gerhard Müller[a]

[a] *Technical University of Munich, Chair of Structural Mechanics, Arcisstr. 21, 80333 Munich, Germany*
[b] *KU Leuven, Campus Diepenbeek, Department of Mechanical Engineering, Wetenschapspark 27, B-3590 Diepenbeek, Belgium*
[c] *KU Leuven, Department of Mechanical Engineering, Celestijnenlaan 300, B-3001 Leuven, Belgium*
[d] *Siemens Industry Software, Simulation and Test Solutions, Interleuvenlaan 68, B-3001 Heverlee, Belgium*
[e] *Flanders Make, Core Lab DMMS*

Abstract

The frequency response of vibro-acoustic systems can be improved by using various forms of damping materials. Their material properties are typically varying with the excitation frequency and are introduced by one or multiple complex-valued functions. Numerical models of such systems are typically large and require efficient solving strategies. In this contribution, a workflow to reduce the numerical complexity of systems containing frequency-dependent damping materials is presented. The functions modeling the material's frequency-dependent behavior are approximated in rational form and the resulting transfer function is used in a Krylov based moment matching method. The approximation is performed automatically using the adaptive Antoulas-Anderson algorithm. As robust and efficient automatic reduction algorithms are vital for an efficient design process of vibro-acoustic structures, we also show an adaptive procedure to automatically find a reasonably sized reduced model for a given system under a certain tolerance. The algorithms are tested for two forms of damping materials common in vibro-acoustic systems: poroelastic materials following the Biot theory and a constrained layer damping material.

Keywords: Higher-order Krylov subspace, Nonlinear damping, Adaptive model order reduction, Vibro-acoustic systems

1. Introduction

The reduction of unwanted noise and vibration is a key issue in the design of vehicles and machines in order to ensure a safe and comfortable operation. Many of these structures are required to withstand high loads but at the same time have a low weight.

*Corresponding author
Email address: quirin.aumann@tum.de (Quirin Aumann)

However, materials with a high stiffness to mass ratio, such as fiber reinforced composites, are not optimal regarding their vibrational properties. The interaction between vibrating structural parts and the surrounding acoustic fluid can cause noise, making the use of a vehicle or machine uncomfortable for passengers or operators, while material fatigue can affect parts of the structure vibrating constantly with relatively high amplitudes, leading to safety issues. Various methods, both active and passive, to reduce unwanted noise and vibrations exist [1–3] and are an important part of the design in many fields of engineering. The effect of energy dissipation mechanisms is typically depending on the excitation frequency of the vibro-acoustic system and is often represented by frequency-dependent material properties [4]. Such material models exist, for example, for constrained layer damping [5, 6] or poroelastic materials described by the Biot theory [7–10].

The finite element method (FEM) is frequently employed in the numerical discretization of mathematical models of vibro-acoustic problems in the low to mid frequency range. In such a setting, the effects of the frequency-dependent materials are often modeled by a combination of scalar functions and constant matrices. In order to be able to resolve all wave phenomena correctly, a fine spatial discretization is required, often leading to very large models with high memory requirements and long computation times. To be able to solve vibro-acoustic problems under reasonable computational effort, different model order reduction methods, for example based on rational interpolation, have been established. They reduce the size of the original numerical model by projecting it onto a lower dimensional subspace using an appropriate reduction basis [11]. Projection-based model order reduction has been successfully applied to different kinds of physical systems in general and also to vibro-acoustic systems [12–15]. Vibro-acoustic systems are typically described by differential equations of second order. Principally it is possible to convert a vibro-acoustic system to an equivalent first-order system of larger size and to employ one of the many available model order reduction methods for first-order systems. Apart from increasing the computational complexity of the original model, which may be prohibiting in some cases, it is desirable for many applications to retain the second-order structure for a reduced order model. A reduced order model with the original matrix structure may preserve spectral properties and allows a physical interpretation of its matrices. If the reduced order model is coupled to other systems, preserving the matrix structure is beneficial as the same coupling conditions for the full and the reduced order models can be applied [16].

However, classic reduction methods have to be adapted in order to consider the behavior of frequency dependent materials also in reduced space. If the damping mechanism can be described by analytic functions, a reduced system of the same structure as the original system can be computed by considering the derivatives of the frequency-dependent functions in the creation of the reduction basis [17]. Such strategies have been applied to vibro-acoustic systems in [12], where a quadratic term in the system excitation has been considered. In extension to the iterative rational Krylov algorithm IRKA [18], general forms of frequency-dependent nonlinear terms in the transfer function have been considered in [19], where optimal expansion points for a rational interpolation of the system's transfer function are iteratively found using the Loewner framework [20]. An analytic derivative of the transfer function is required for this structure-preserving method. The Loewner framework itself has also been used for model order reduction [21]. Contrary to the other model order reduction methods summarized in this paragraph, it only utilizes input and output data of a system and does not require access to the sys-

tem states or its matrices. Operator inference is a data-driven approach constructing a reduced order approximation of the system operators from input and output data and trajectories of the system states and can therefore also be employed for systems with frequency-dependent material properties [22, 23]. Other data-driven methods, such as proper orthogonal decomposition (POD) [24] or dynamic mode decomposition (DMD) [25] can also be employed. Note, that a large amount of data from the full-scale numerical model can be required for an efficient application of data-driven methods. The mode displacement method, typically used for classically damped systems, can be extended to vibro-acoustic systems with nonlinear damping behavior as presented in [14]. The modes of such systems have been used to compute the coefficients for a Padé expansion around specific frequencies of interest in [26, 27]. A method to find the eigenvalues of systems with nonlinear frequency dependency using a linearized matrix pencil is presented in [28]. Here, the nonlinear contributions are approximated by the adaptive Antoulas-Anderson (AAA) algorithm [29] and the matrix pencil is augmented by the higher order terms of the approximation, changing the original structure of the problem. A classic model order reduction method is to use an Arnoldi method to approximate the original system's transfer function and some of its derivatives around certain frequency shifts. Arnoldi methods for second-order systems [30, 31] have been used in [32] to compute a reduction basis for systems with frequency-dependent damping. Here, the frequency-dependent functions are approximated by a Taylor series which is truncated after the quadratic term in order to fit the second order structure of the Arnoldi method. Again, analytic derivatives are required for this approach.

In the following, we present a workflow to compute reduced order models for systems whose transfer functions contain functions which are nonlinear regarding the driving frequency. The gist of the method is a reformulation of the system's transfer function, such that it contains only polynomial terms up to a certain order, and to use a Krylov space of the same order to compute a reduction basis. In the first step, AAA [29] is used to automatically find a rational approximant of the non-polynomial function. Following, a series expansion of the approximant about the same shift that shall be used for computing the Krylov subspace is performed, leading to a polynomial representation of the approximated function. After replacing the original function in the transfer function by this approximation, the modified transfer function contains only polynomial terms. A series expansion about an expansion point can easily be computed from this representation, leading to a higher order Krylov subspace, as shown, for example, in [17, 33]. Depending on the desired accuracy, the resulting polynomial, which is determining the order of the employed Krylov subspace, can be truncated at an arbitrary order. One or more of these subspaces are then used to compute the projection basis for model order reduction. A similar polynomial approximation of the transfer function terms can also be obtained using, for example, a Taylor expansion [32]. Contrary to this Taylor-based approach, AAA requires only function evaluations to find a rational approximant and neither analytic expressions nor derivatives of the nonlinear functions are required. Therefore, damping effects described by data which has been obtained from measurements can potentially be used in this procedure. Additionally, the proposed workflow is directly applicable to any problem exhibiting a frequency dependency in the transfer function as long as this function can be represented by a AAA approximant of appropriate order. Nonlinear effects not described by a combination of scalar functions and constant matrices are not in the scope of this workflow.

In order to efficiently use reduced order models in a design process or in optimization tasks, automatic methods to reduce the original model under a specified accuracy are required. The approximation error of the reduced system is typically unknown and has to be estimated, as the solution of the full problem is assumed to be unavailable prior to the simulation. Different kinds of error estimators or bounds exist in literature and are the basis for adaptive methods, which find a reasonable reduced order and locations for expansion points in an iterative procedure. Such heuristic algorithms have been proposed, for example, in [32, 34–39]. The structure of these algorithms is similar to reduced basis (RB) approaches, where suitable locations for expansion points are often obtained from a greedy method [40, 41]. Reduced basis methods have also been successfully applied to vibro-acoustic systems in, for example, [42]. Error estimators required for adaptive algorithms are often based on residual expressions or the comparison of multiple reduced models having different orders or with different expansion points [35, 43–45]. Algorithms employing such techniques have been found suitable to reduce systems with frequency-dependent material properties: The residuals of the intermediate reduced models of systems with general nonlinear damping effects are used as an error estimate in [46]; two independent reduced models of vibro-acoustic systems with poroelastic material damping are computed based on different expansion points and compared to obtain an estimate for the approximation error in [47]. Most of the mentioned algorithms are based on increasing the size of the reduced order model between iterations. Similarly, we suggest an adaptive algorithm to find a reasonable distribution of expansion points using a greedy method, in order to compute an appropriately sized reduced order model valid in a specified frequency range. Additionally to increasing the size of the reduced order model, the algorithm also increases the order of the employed Krylov subspaces adaptively. This can increase the accuracy of the resulting reduced order model without enlarging its size. The iterative algorithm estimates the reduction error by comparing the individual subspaces around the expansion points as well as the transfer functions of reduced order models coming from subsequent iterations.

Combining the reformulation of the frequency-dependent function with the adaptive algorithm results in an intrusive and structure-preserving model order reduction strategy. The workflow is started by providing a frequency range in which the reduced order model should be valid, the full-order model with the frequency-dependent functions given either explicitly or as data points, and a desired approximation accuracy. The following steps are then performed without user input, particularly: (i) approximating the frequency-dependent functions using AAA and considering them in the computation of the Krylov spaces; (ii) estimating an appropriate order of the involved Krylov spaces and the size of the final reduced order model. We therefore refer to this workflow as being automatic.

The remainder of the article is structured as follows: The reduction method based on higher-order Krylov subspaces and the AAA algorithm is presented in section 2. The adaptive algorithm is presented in section 3. Section 4 contains numerical experiments showing the performance of the model order reduction method and the adaptive algorithm by the example of two vibro-acoustic systems. Concluding remarks are drawn in section 5.

2. Model order reduction for systems with nonlinear frequency dependency

2.1. Model order reduction using a higher-order Krylov subspace

We first revisit a method for model order reduction using a higher-order Krylov subspace, originally proposed in [33]. It can be applied to single input, single output (SISO) dynamical systems with a maximum derivative order of k. Such systems of differential equations have the following form

$$\Sigma : \begin{cases} \mathbf{A}_k \dfrac{\mathrm{d}^k}{\mathrm{d}t^k}\mathbf{x}(t) + \cdots + \mathbf{A}_1 \dfrac{\mathrm{d}}{\mathrm{d}t}\mathbf{x}(t) + \mathbf{A}_0\mathbf{x}(t) = \mathbf{b}u\,(t) \\ y\,(t) = \mathbf{c}^{\mathsf{T}}\mathbf{x}\,(t)\,, \end{cases} \tag{1}$$

with constant system matrices $\mathbf{A}_i \in \mathbb{R}^{n\times n}, i = 0, \ldots, k$, input and output mapping $\mathbf{b}, \mathbf{c} \in \mathbb{R}^n$, state $\mathbf{x}(t) \in \mathbb{R}^n$, and scalar inputs and outputs $u(t), y(t)$. t denotes the time variable. In a vibro-acoustic context, $k = 2$ for classically damped systems and $\mathbf{A}_0$ corresponds to the stiffness matrix, $\mathbf{A}_1$ is the viscous damping matrix, and $\mathbf{A}_2$ is the mass matrix. A transformation to frequency domain yields

$$\Sigma : \begin{cases} \left(\sum_{i=0}^{k} s^i \mathbf{A}_i\right) \tilde{\mathbf{x}}\,(s) = \mathbf{b}\tilde{u}\,(s) \\ \tilde{y}\,(s) = \mathbf{c}^{\mathsf{T}}\tilde{\mathbf{x}}\,(s)\,, \end{cases} \tag{2}$$

with the Laplace transforms of the state $\tilde{\mathbf{x}}(s) \in \mathbb{C}^n$, input $\tilde{u}(s)$, and output $\tilde{y}(s)$. The complex frequency is typically given by $s = \mathrm{i}\omega$, where $\mathrm{i}^2 = -1$ and ω is the driving frequency. The corresponding transfer function is

$$H\,(s) = \mathbf{c}^{\mathsf{T}} \left(\sum_{i=0}^{k} s^i \mathbf{A}_i\right)^{-1} \mathbf{b}. \tag{3}$$

As this transfer function contains only polynomial terms, we will refer to such systems as "polynomial systems" in the remainder. For vibro-acoustic systems and many other types of dynamical systems, n is large and we want to find a reduced system Σ_r of order $r \ll n$ preserving the original system's matrix structure:

$$\Sigma_r : \begin{cases} \left(\sum_{i=0}^{k} s^i \mathbf{A}_{i,r}\right) \tilde{\mathbf{x}}_r\,(s) = \mathbf{b}_r\tilde{u}\,(s) \\ \tilde{y}_r\,(s) = \mathbf{c}_r^{\mathsf{T}}\tilde{\mathbf{x}}_r\,(s)\,. \end{cases} \tag{4}$$

Here, the subscript r denotes a reduced quantity. The reduced model is considered accurate, if its transfer function approximates the original model's transfer function in a certain frequency range of interest; so we require $H_r\,(s) \approx H\,(s)$ for some s. The reduced system's transfer function is given by

$$H_r\,(s) = \mathbf{c}_r^{\mathsf{T}} \left(\sum_{i=0}^{k} s^i \mathbf{A}_{i,r}\right)^{-1} \mathbf{b}_r. \tag{5}$$

This reduced representation can be achieved by projecting the original system onto a lower dimensional subspace using a Petrov-Galerkin projection. Two subspaces $\mathcal{V}_r$, $\mathcal{W}_r$

spanned by two matrices $\mathbf{V}, \mathbf{W} \in \mathbb{C}^{n \times r}$ are required for the projection [11, 12] and are selected, such that

$$\mathbf{W}^{\mathsf{H}} \left(\left(\sum_{i=0}^{k} s^i \mathbf{A}_i \right) \mathbf{V} \tilde{\mathbf{x}}_r (s) - \mathbf{b} \tilde{u} (s) \right) = 0. \tag{6}$$

It follows

$$\tilde{y}_r (s) = \mathbf{c}^{\mathsf{T}} \mathbf{V} \tilde{\mathbf{x}}_r (s) . \tag{7}$$

The reduced vectors and matrices in eq. (4) are thus given by

$$\mathbf{A}_{i,r} = \mathbf{W}^{\mathsf{H}} \mathbf{A}_i \mathbf{V}, \ \mathbf{b}_r = \mathbf{W}^{\mathsf{H}} \mathbf{b}, \ \mathbf{c}_r^{\mathsf{T}} = \mathbf{c}^{\mathsf{T}} \mathbf{V}, \tag{8}$$

where $(\bullet)^{\mathsf{H}}$ denotes the Hermitian transpose of a matrix. For symmetric systems (2), setting $\mathbf{W} = \mathbf{V}$ preserves the symmetry in the reduced space [48]. If both subspaces $\mathcal{V}_r$, $\mathcal{W}_r$ are closed under conjugation, a real valued representation of the reduced matrices and vectors in eq. (4) can be obtained [11].

A classic choice for the projection subspaces are Krylov spaces [11]. For systems with $k = 2$ given by eq. (2), a second-order Krylov subspace can be employed [49, 50]. Lin et al. [33] extended this idea for an arbitrary order k. Both methods are special cases of a general structure preserving reduction framework introduced by Beattie and Gugercin [17].

A kth order Krylov space is defined by k matrices $\mathbf{Z}_1, \ldots, \mathbf{Z}_k$ and a vector $\mathbf{v}_0$ and is spanned by the recursive vector sequence

$$\begin{aligned} \mathbf{r}_0 &= \mathbf{v}_0 \\ \mathbf{r}_1 &= \mathbf{Z}_1 \mathbf{r}_0 \\ \mathbf{r}_2 &= \mathbf{Z}_1 \mathbf{r}_1 + \mathbf{Z}_2 \mathbf{r}_0 \\ &\vdots \\ \mathbf{r}_{r-1} &= \mathbf{Z}_1 \mathbf{r}_{r-2} + \mathbf{Z}_2 \mathbf{r}_{r-3} + \cdots + \mathbf{Z}_k \mathbf{r}_{r-k-1}. \end{aligned} \tag{9}$$

Here, $\mathbf{Z}_1 = -\mathbf{A}_0^{-1} \mathbf{A}_1$, $\mathbf{Z}_2 = -\mathbf{A}_0^{-1} \mathbf{A}_2$, $\ldots$, $\mathbf{Z}_k = -\mathbf{A}_0^{-1} \mathbf{A}_k$, and $\mathbf{v}_0 = -\mathbf{A}_0^{-1} \mathbf{b}$. The resulting space

$$\mathcal{K}_r^{(k)} (\mathbf{Z}_1, \ldots, \mathbf{Z}_k, \mathbf{v}_0) = \operatorname{span} \{ \mathbf{r}_0, \mathbf{r}_1, \ldots, \mathbf{r}_{r-1} \} \tag{10}$$

is called the rth Krylov subspace of order k [33]. An orthonormal basis $\mathbf{V}$ of the Krylov space $\mathcal{K}_r^{(k)}$ is found using, for example, an Arnoldi procedure [31, 49, 51] and can be used for projection as in eq. (6) [30]. The subspace for basis $\mathbf{W}$ is found similarly by setting $\mathbf{Z}_1 = \left(-\mathbf{A}_0^{\mathsf{T}}\right)^{-1} \mathbf{A}_1^{\mathsf{T}}$, $\mathbf{Z}_2 = \left(-\mathbf{A}_0^{\mathsf{T}}\right)^{-1} \mathbf{A}_2^{\mathsf{T}}$, $\ldots$, $\mathbf{Z}_k = \left(-\mathbf{A}_0^{\mathsf{T}}\right)^{-1} \mathbf{A}_k^{\mathsf{T}}$, and $\mathbf{v}_0 = \left(\mathbf{A}_0^{\mathsf{T}}\right)^{-1} \mathbf{c}$. The resulting reduced model matches the first r moments of the original transfer function around $s_0 = 0$. If all system matrices $\mathbf{A}_i$ are symmetric and this symmetry is preserved in the reduced order model by choosing $\mathbf{W} = \mathbf{V}$, the first $2r$ moments are matched [30]. Often the approximation around a specified frequency $s_0 \neq 0$ is desired. To achieve this, the transfer function is rewritten to include the shift s_0

$$H (s) = \mathbf{c}^{\mathsf{T}} \left(\sum_{i=0}^{k} (s - s_0)^i \widehat{\mathbf{A}}_i \right)^{-1} \mathbf{b}, \tag{11}$$

with $\widehat{\mathbf{A}}_i = \sum_{j=i}^{k} \binom{j}{i} \mathbf{A}_k s_0^{j-i}$. The binomial operator is given by $\binom{j}{i} = \frac{j!}{i!\,(j-i)!}$. The choice of subspace size r and location of the shift has a large influence on the approximation quality of a reduced model. To increase the reduced model's accuracy for a wide range of frequencies, it can be beneficial to not only increase the size of the Krylov subspace, but to combine multiple subspaces with different shifts s_0 in a global basis [43, 52]. Adding a new shift to the projection basis involves the solution of up to two linear systems of equations of order n. Increasing the order at an already established shift only requires matrix vector products if the factorization of $\mathbf{Z}_0$ is stored for each shift and a suitable Arnoldi strategy is chosen [49].

2.2. Dynamic systems with nonlinear frequency dependency

We now consider dynamical systems having general nonlinearities regarding the excitation frequency $s = \mathrm{i}\omega$. The nonlinearity is introduced by l complex-valued scalar functions $\phi_j(s)$, $j = 1, \ldots, l$, which are assumed to be known in the following, and are applied to the system according to l corresponding constant matrices $\mathbf{G}_j \in \mathbb{R}^{n \times n}$. In the frequency domain, such systems are given by

$$\Sigma : \begin{cases} \left(\sum_{i=0}^{k} s^i \mathbf{A}_i + \sum_{j=1}^{l} \phi_j(s)\, \mathbf{G}_j \right) \tilde{\mathbf{x}}(s) = \mathbf{b}\tilde{u}(s) \\ \qquad\qquad\qquad\qquad \tilde{y}(s) = \mathbf{c}^{\mathsf{T}} \tilde{\mathbf{x}}(s), \end{cases} \tag{12}$$

with the corresponding transfer function

$$H(s) = \mathbf{c}^{\mathsf{T}} \left(\sum_{i=0}^{k} s^i \mathbf{A}_i + \sum_{j=1}^{l} \phi_j(s)\, \mathbf{G}_j \right)^{-1} \mathbf{b}. \tag{13}$$

The application of the Krylov method described in the last section requires a series expansion of the transfer function in order to incorporate all effects of the nonlinear function; see, for example, Theorem 2 in [17]. As these factors may not be easy to obtain for some functions $\phi_i(s)$ in eq. (12), we want to find a representation of the system approximating the nonlinear function with a polynomial of degree d. This leads to a system with the transfer function

$$H(s) \approx \check{H}(s) = \mathbf{c}^{\mathsf{T}} \left(\sum_{i=0}^{k} s^i \mathbf{A}_i + \sum_{\ell=0}^{d} s^\ell \check{\mathbf{G}}_\ell \right)^{-1} \mathbf{b}. \tag{14}$$

In this case, each matrix $\check{\mathbf{G}}_\ell$ incorporates the series expansion factors of the original function for the corresponding order; the strategy to obtain these factors is presented in the following section. If multiple functions $\phi(s)$ are approximated, $\check{\mathbf{G}}_\ell$ is a linear combination of all matrices $\mathbf{G}_j$ and their expansion factors corresponding to order ℓ. The modified transfer function eq. (14) can be shifted similarly to eq. (11), if an approximation around $s_0 \neq 0$ is desired. Using a Krylov subspace of order $\max\{k, d\}$ allows considering also higher-order terms of the polynomial, increasing the frequency range where an accurate approximation of the original function $\phi(s)$ is acquired. While typically $k = 2$ for vibro-acoustic systems, d can be arbitrary and depends on the function

to be approximated. Note, that the maximum polynomial order in eq. (14) determines the order of the employed Krylov space. Although the structure of the original transfer function (13) is reformulated to eq. (14) to be able to apply the Krylov method from section 2.1, the projection is performed on the original matrices from eq. (13). Thus the original structure of the full-order model is preserved.

A similar approach has been proposed by Xie et al. [32] which employs expansion factors obtained from a Taylor series approximating a nonlinear function. Contrary to the workflow presented here, this expansion is truncated after the quadratic term in order to use the second-order Krylov subspace from Bai and Su [49]. However, this yields reduced order models potentially showing a stagnating approximation quality with increasing distance from the frequency shift. If the quadratic approximation of $\phi(s)$ is not able to represent the original function well, increasing the order r does not improve the approximation quality. A possible remedy is establishing new expansion points, but this involves solving at least one linear system of full order n per shift.

Therefore, we evaluate the benefits of applying higher-order Krylov subspaces which are able to consider higher-order series expansion factors. This potentially increases the frequency range in which $\phi(s)$ is approximated with high accuracy, thus requiring a lower reduced order r and less expansion points for an accurate reduced order model. Additionally, the number of required matrix factorizations is independent of the order of the Krylov subspace k. Increasing order k and size r of the subspace requires only matrix vector multiplications.

2.3. Automatic approximation of frequency dependent nonlinearities

In the following, we outline a workflow to automatically find approximations to the scalar functions $\phi_i(s)$ and add them to a shifted transfer function given by eq. (14). The adaptive Antoulas-Anderson (AAA) algorithm [29] is used to find a representation for $\phi_i(s)$ in a frequency range of interest, given data points rather than an analytic function. It can therefore also be applied in cases, where only discrete data, for example from measurements, is available. As AAA is an adaptive algorithm, it ensures a certain accuracy of the approximant upon convergence without the need for manually optimizing its order or the location of the support points. Therefore it can be used in the automatic approximation of $\phi_i(s)$ given only the function values, a tolerance, and a maximum order. AAA has been successfully used to solve nonlinear eigenvalue problems [28] and to linearize dynamic systems with nonlinear frequency dependency [16, 53]. Such linearization allows the direct use of standard model order reduction methods, but the system's structure is changed and the order is increased from n to $n(d+1)$ prior to the reduction, d being the maximum polynomial order of the nonlinear terms.

In the following, the nonlinear functions in eq. (12) are approximated up to an arbitrary order d and a Krylov subspace of the same order is subsequently used to find a suitable reduction basis. An enlargement of the original system is not necessary and the reduced system retains the structure of the original system. Contrary to approximating the nonlinear frequency contributions with, for example, a Taylor series, this method can be employed without the need for analytic derivatives. Therefore it can be applied to different kinds of problems with an affine representation of frequency dependent behavior without the need of problem-specific changes.

AAA, originally introduced by Nakatsukasa et al. [29], finds a rational approximation $r_i(s)$ of $\phi_i(s)$ in barycentric form

$$\phi_i(s) \approx r_i(s) = \sum_{j=1}^{m} \frac{w_{i,j} f_{i,j}}{s - s_{i,j}} \Bigg/ \sum_{j=1}^{m} \frac{w_{i,j}}{s - s_{i,j}}\,, \tag{15}$$

where $m \geq 1$ is the order of approximation, $w_{i,j}$ are weights, $f_{i,j}$ are data points, and $s_{i,j}$ are support points. Note, that eq. (15) can also be expressed as a quotient of polynomials. In the case of a successful AAA iteration, these polynomials are each of degrees $m-1$ [29]. The support points are found using a greedy method and the weights are obtained by solving a least-squares problem [29]. Following [28], the barycentric form of $r_i(s)$ can be written in matrix notation as

$$\begin{gathered} r_i(s) = \mathbf{p}_i \left(\mathbf{R}_i + s\mathbf{T}\right)^{-1} \mathbf{q} \\ \text{with } \mathbf{p}_i = \begin{bmatrix} w_{i,1} f_{i,1} & \cdots & w_{i,m} f_{i,m} \end{bmatrix},\ \mathbf{q} = \begin{bmatrix} 1 & 0 & \cdots & 0 \end{bmatrix}^{\mathsf{T}}, \\ \mathbf{R}_i = \begin{bmatrix} w_{i,1} & w_{i,2} & \cdots & w_{i,m-1} & w_{i,m} \\ -s_{i,1} & s_{i,2} & & & \\ & -s_{i,2} & \ddots & & \\ & & \ddots & s_{i,m-1} & \\ & & & -s_{i,m-1} & s_{i,m} \end{bmatrix},\ \mathbf{T} = \begin{bmatrix} 0 & 0 & \cdots & 0 & 0 \\ 1 & -1 & & & \\ & 1 & \ddots & & \\ & & \ddots & -1 & \\ & & & 1 & -1 \end{bmatrix}. \end{gathered} \tag{16}$$

Shifting the system about s_0 results in

$$r_i(s) = \mathbf{p}_i \left(\mathbf{I} - (s - s_0)\,\widehat{\mathbf{R}}_i\right)^{-1} \hat{\mathbf{q}}_i, \tag{17}$$

with $\widehat{\mathbf{R}}_i = -\left(\mathbf{R}_i + s_0\mathbf{T}\right)^{-1}\mathbf{T}$, $\hat{\mathbf{q}}_i = \left(\mathbf{R}_i + s_0\mathbf{T}\right)^{-1}\mathbf{q}$ and identity $\mathbf{I}$. As m is typically small, the computational cost of the matrix operations required for shifting the system can be neglected. In the vicinity of s_0, the matrix inverse in eq. (17) can be approximated with a Neumann series

$$r_i(s) = \mathbf{p}_i\hat{\mathbf{q}}_i + \mathbf{p}_i \left((s - s_0)\,\widehat{\mathbf{R}}_i\right)\hat{\mathbf{q}}_i + \mathbf{p}_i \left((s - s_0)\,\widehat{\mathbf{R}}_i\right)^2 \hat{\mathbf{q}}_i + \ldots. \tag{18}$$

To obtain the transfer function of the shifted system (14) including the nonlinearity, we shift the AAA approximations about the same shift s_0 as the polynomial terms and truncate the Neumann series after the dth term. After inserting the approximations into the transfer function and shifting everything, we arrive at a shifted variant of eq. (14)

$$H(s) = \mathbf{c}^{\mathsf{T}} \left(\sum_{i=0}^{k} (s - s_0)^i\, \widehat{\mathbf{A}}_i + \sum_{\ell=0}^{d} (s - s_0)^\ell\, \widehat{\tilde{\mathbf{G}}}_\ell\right)^{-1} \mathbf{b}, \tag{19}$$

with $\widehat{\mathbf{A}}_i = \sum_{j=i}^{k} \binom{j}{i} \mathbf{A}_k s_0^{j-i}$, $\widehat{\tilde{\mathbf{G}}}_\ell = \sum_{j=1}^{l} \mathbf{p}_j \widehat{\mathbf{R}}_j^\ell \hat{\mathbf{q}}_j \mathbf{G}_j$. Now, the $\max\{k, d\}$th Krylov subspace can be found using an Arnoldi method as described in section 2.1.

3. Automatic model order reduction with higher-order Krylov subspaces

In order to find an accurate reduced order model with the proposed framework, the locations and orders of the expansion points need to be set properly. This cannot always be achieved without prior knowledge of the full system's response, so adaptive methods determining reasonable locations and orders of expansion points are required. Such methods should find a reasonably small reduced order model without being too computationally demanding. For a successful error assessment, the exact relative approximation error of the reduced model's transfer function compared to the original system

$$\varepsilon(\omega) = \frac{|H(\mathrm{i}\omega) - H_r(\mathrm{i}\omega)|}{|H(\mathrm{i}\omega)|} \tag{20}$$

is required for frequencies ω where the reduced order model should be valid. As this error is not available without the solution of the full system, which is not desirable to compute, it has to be estimated as $\hat{\varepsilon}(\omega) \approx \varepsilon(\omega)$. In the following algorithm, we use an error estimation technique presented by Grimme in [43] to identify frequency regions where the approximation quality of the reduced order model is not sufficient. The approximation error is estimated by the difference of the transfer functions of two reduced order models approximating the same full order system but having different expansion points, reduced orders, or are computed using different orders of Krylov subspaces. Their transfer functions are denoted by $H_{r,1}$ and $H_{r,2}$ and the estimated error is given by

$$\hat{\varepsilon}(\omega) = \frac{|H_{r,1}(\mathrm{i}\omega) - H_{r,2}(\mathrm{i}\omega)|}{|H_{r,1}(\mathrm{i}\omega)|}. \tag{21}$$

If the difference between the transfer functions of such two models is sufficiently small with respect to a specified tolerance, it is assumed that the original system response is approximated well by both reduced models in the considered frequency range. Further increasing the order has presumably little effect on the approximation quality. The difference between the two compared reduced order models has to be chosen adequate, such that the two models are different enough from each other and the error is not underestimated.

In the following, we present an adaptive method for automatic model order reduction of systems with frequency-dependent properties. It computes a reduced order model valid in a specified frequency range without requiring a priori knowledge of the original model's solution. The algorithm is based on increasing the order of the employed Krylov spaces and enlarging the size of the reduced model until the estimated error in the frequency range of interest is below a defined threshold. The reduced order is increased by adding new expansion points. Appropriate locations for new expansion points are found using a greedy method. The method to obtain an approximation for frequency dependent functions described in section 2 is used to obtain all involved reduction bases. The complete algorithm is given in pseudo code in Algorithm 3.1.

The adaptive algorithm starts with one or more locations for initial expansion points distributed in the frequency range of interest provided by the user. For each expansion point, a local subspace and the corresponding reduced order model is computed. Subsequently, the approximation error in the frequency range between each pair of adjacent expansion points is estimated according to eq. (21). If both local reduced order models

Algorithm 3.1 Adaptive reduction algorithm.

Require: Original system Σ, initial expansion points $s_{0,i},\ i = 1, \ldots, n_s$ with corresponding initial sizes $r_{0,i}$ and subspace orders k_i, frequency range $\varsigma = [\omega_{\min}, \omega_{\max}]$, minimum and maximum subspace order $k_{\min}$,$k_{\max}$, order increment k_{incr}; tolerance ε_{tol}, maximum size of the reduced system $r_{\max}$

Ensure: Reduced system Σ_r

while $\max_{\omega \in \varsigma} (\hat{\varepsilon}(\omega)) > \varepsilon_{\text{tol}}$ **and** $r_{\text{glob}} < r_{\max}$ **do**
  Compute $\Sigma_{r,i}$ for each $s_{0,i}$ and corresponding k_i
  Compute $\hat{\varepsilon}_{ij}(\omega)$ for each pair of adjacent $s_{0,i}$ and $s_{0,j}$ following eq. (21)
  if $\hat{\varepsilon}_{ij}(\omega) < \varepsilon_{\text{tol}}$ **then**
    Combine subspaces for $\Sigma_{r,i}$ and $\Sigma_{r,j}$
    Flag combined subspaces inactive
  end if
  Compute global subspace from all active local subspaces and reduce Σ
  Update r_{glob}
  Compute global error estimator $\hat{\varepsilon}(\omega)$ in range ς
  Find $s_{0,j}$ whose location is next to $\max \hat{\varepsilon}(\omega)$
  if $k_j < k_{\max}$ **then**
    $k_j = k_j + k_{\text{incr}}$
  else
    Add new expansion point at $\mathrm{i}\omega_{\text{new}}$, $\omega_{\text{new}} = \max_{\omega \in \varsigma} \hat{\varepsilon}_1(\omega)$ and initialize with r_0, $k_{\min}$
  end if
end while
Compute Σ_r with the global subspace

have, under a specified tolerance, similar transfer functions in this region, the reduced model is considered sufficiently accurate in this frequency region and both local subspaces are combined to a single subspace. The involved subspaces are now flagged as inactive. This means the subspace orders associated to the respective expansion points are not increased anymore, as this would not lead to a better approximation in the area between them. After all pairs of subspaces have been processed, a global reduction basis is computed from all active local subspaces and $\hat{\varepsilon}(\omega)$ is evaluated for the complete frequency range of interest. If the estimated error is higher than the specified tolerance, the subspace order k of the subspace with the corresponding expansion point located next to the highest estimated error is increased by k_{incr}. If the highest estimated error is next to an expansion point with maximum order $k_{\max}$, a new shift is introduced here. Also if all local subspaces are combined and flagged as inactive and the estimated error is higher than the specified tolerance, a new expansion point is established at the location where $\hat{\varepsilon}(\omega)$ has its maximum value. If the estimated error is below the defined tolerance or the size of the global reduced order model is larger than a specified value $r_{\max}$, the final reduced model is computed using the current global basis.

4. Numerical experiments

The combination of a higher-order Krylov subspace using series expansion factors obtained from AAA is evaluated by the example of two numerical models of different complexity incorporating frequency dependent material properties. All following numerical experiments were conducted on single nodes of the MPI Magdeburg's computing cluster Mechthild. Each node is equipped with two Intel® Xeon® Silver 4110 (Skylake) CPUs with eight cores per CPU and a maximum clock rate of 3.0 GHz. 192 GB memory are available per job. The algorithms have been implemented and run using Matlab® R2020b. All code and data used to produce the results in the following section is available from doi:10.5281/zenodo.6225761 [54].

The complex-valued reduction bases used in the following experiments are obtained by single-sided projection regarding the system input, i.e. setting $\mathbf{W} = \mathbf{V}$ in eq. (8). In order to assess the approximation quality of the reduced models, the relative difference between the absolute values of original and reduced transfer functions eq. (20) is evaluated. To be able to compare multiple reduced models at once, the relative error regarding original and reduced transfer functions under an approximation of the $\mathcal{L}_\infty$-norm

$$\varepsilon = \frac{\max\limits_{\omega\in[\omega_{\min},\omega_{\max}]} \|H(\mathrm{i}\omega) - H_r(\mathrm{i}\omega)\|_2}{\max\limits_{\omega\in[\omega_{\min},\omega_{\max}]} \|H(\mathrm{i}\omega)\|_2} \approx \frac{\|H - H_r\|_{\mathcal{L}_\infty}}{\|H\|_{\mathcal{L}_\infty}}, \tag{22}$$

is used to obtain a single value showing the approximation quality of a reduced model.

4.1. Viscoelastic sandwich beam model

As first example, we consider a system with one frequency dependent function. It models a symmetric sandwich beam with length $l = 0.21$ m, consisting out of two layers of cold rolled steel surrounding a viscoelastic ethylene-propylene-diene core [6]. The beam is clamped at one side, a sketch is given in fig. 1.

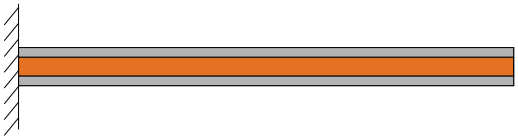

Figure 1: A sketch of the sandwich beam with viscoelastic core. The steel face sheets are depicted gray, the viscoelastic core orange.

The system is discretized using finite elements and has an order of $n = 3360$; the matrices have been taken from [55]. Due to the relatively small size of the original model, the computation times are not considered in this example. The beam is excited by a single load at its free end and the displacement is measured at the same location; the frequency response function is given in fig. 3. The dissipation behavior of the constrained layer damping can be described by a fractional derivative (FD) model extending a Zener model and is added by a nonlinear function depending on s [5, 56]. The resulting system's transfer function is of the shape

$$H(s) = \mathbf{c}^\mathsf{T}\left(s^2\mathbf{A}_2 + \mathbf{A}_0 + \frac{G_0 + G_\infty(s\tau)^\alpha}{1 + (s\tau)^\alpha}\mathbf{G}_1\right)^{-1}\mathbf{b}, \tag{23}$$

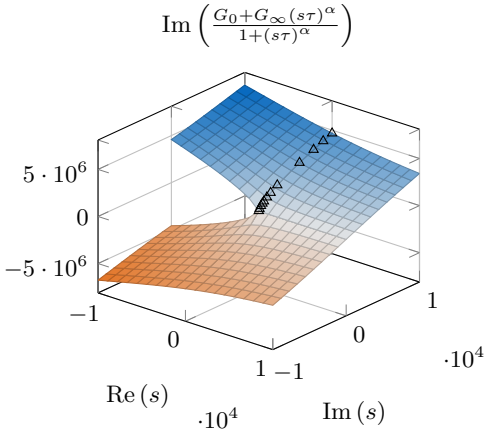

(a) Original function with support points chosen by AAA (triangles).

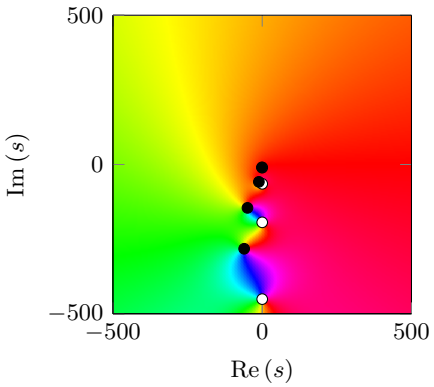

(b) Section of the phase portrait [57] of the approximant with poles (white dots) and zeros (black dots).

Figure 2: The complex-valued function governing the fractional derivative damping model.

where $\mathbf{A}_0, \mathbf{G}_1$ are the stiffness distributions of the elastic and viscoelastic parts and $\mathbf{A}_2$ is the mass distribution of the system. The parameters for the FD model are $G_0 = 350.4\,\text{kPa}$, $G_\infty = 3.062\,\text{MPa}$, $\tau = 8.230\,\text{ns}$, $\alpha = 0.675$. The FE model is evaluated in the frequency range $\omega = [10, \ldots, 10000]$. 100 function evaluations on points distributed equidistantly on the imaginary axis in the range $\mathrm{i}\omega$ are used to obtain a AAA approximation of the FD model function, as only the function values in this region are of interest for the application. AAA converges at an order of 12 given a tolerance of $1{\cdot}10^{-14}$; the original function and the support points chosen by AAA are given in fig. 2a. A section of the phase portrait [57] of the approximant is plotted in fig. 2b. It can be seen, that the branch cut along the negative real axis is not present in the approximated function. This is, however, not hindering the application of the approximant in this setting, as only the behavior of the function along the imaginary axis needs to be approximated. The poles and zeros of the approximant are alternating in direction of the negative imaginary axis. AAA converges without computing spurious poles, so the cleanup step proposed in [29] is not performed. The application of AAA to functions with branch cut singularities, as the FD model function, has been recently examined in [58].

Figure 3 shows the impact of approximating and expanding the frequency dependent function in eq. (23) to the result of the transfer function. Here, the function $\phi(s)$ is approximated using AAA and expanded about the shift $s_0 = 100\mathrm{i}$ up to order k. Orders higher than k are truncated. While increasing the truncation order leads to a wider range of accurate approximation, all approximated transfer functions substantially deviate from the original with increasing distance to the frequency shift. However, a reduced order model computed using a Krylov space about this shift is able to approximate the full order model's transfer function over the complete considered frequency range, as will be shown in the following.

The reduction basis is computed using the same expansion point $s_0 = 100\mathrm{i}$ near the first peak in the original transfer function and using different expansion orders k. For $k < 2$ a second-order Krylov subspace is used for computing the reduction basis in order

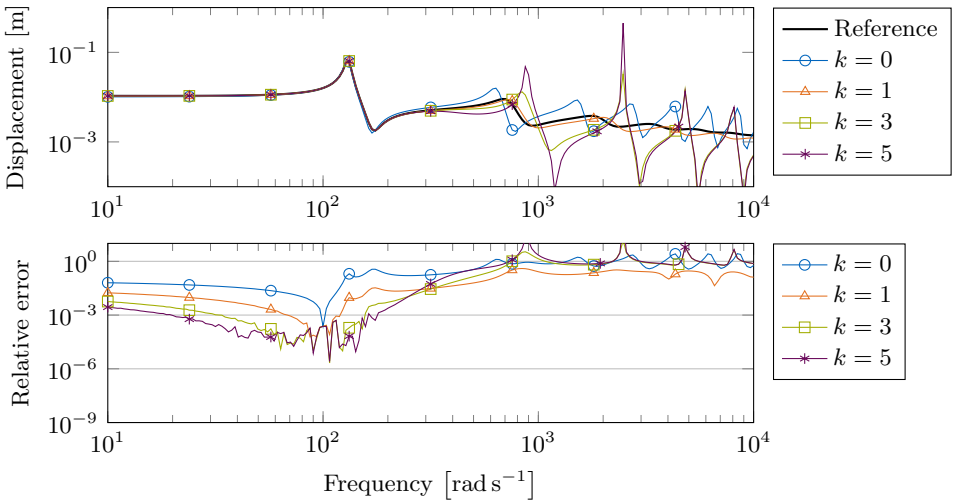

Figure 3: The sandwich beam model's transfer function, where the frequency dependent function governing the fractional derivative damping model is approximated by expansions of different orders shifted about $s_0 = 100\mathrm{i}$.

to incorporate the effects linked to the matrix $\mathbf{A}_2$ in eq. (23). However, the expansion of the AAA approximant of the FD function is truncated at k. The benefit of a higher subspace order k can be observed in the relative approximation error plot in fig. 4. Here, the original model is reduced to $r = 15$ using Krylov spaces of different orders k. The relative errors of all models are low in the vicinity of the shift. The approximation error of the reduced order model computed by linearizing the frequency-dependent function (i.e. $k = 0$) is substantially higher in the considered frequency region than for the models considering higher-order expansion factors. Note, that the approximation quality of the reduced order model is better than the approximation of the frequency dependent function regarding the full order model shown in fig. 3.

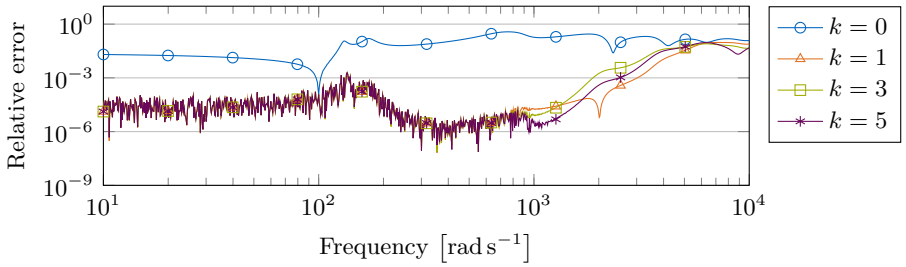

Figure 4: Relative approximation error of the sandwich beam model. Approximation with different orders k of the Krylov subspace expanded about $s_0 = 100\mathrm{i}$ with reduced order $r = 15$.

Increasing the reduced order r yields reduced models being sufficiently accurate for

all values of $k > 0$. Figure 5 shows the approximated relative $\mathcal{L}_\infty$-errors for reduced models of different sizes r compared to the order of the respective Krylov subspace k. All reduced models with $k > 0$ achieve a reasonable approximation quality in the desired frequency range, suggesting that the automatic approximation of the FD model function in eq. (23) is successful. Choosing a higher subspace order k tends to lead to an earlier drop in the maximum relative error, showing the potentially higher accuracy of models based on a higher k given a certain size of the reduced order model r. The observation that all models with $k > 0$ reach a similar accuracy shows that the damping introduced by the FD model can be approximated well by a linear function. However, a constant function cannot capture the behavior of the FD model over the complete frequency range.

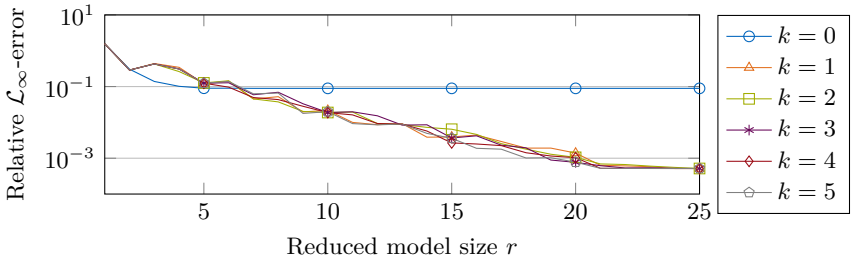

Figure 5: Relative errors in the frequency range $\omega = [10, \ldots, 10000]$ of reduced models of the sandwich beam regarding different sizes r and Krylov subspace orders k. All subspaces are expanded around $s_0 = 100\mathrm{i}$.

4.2. Poroelastic material coupled to an acoustic cavity

We now consider a three-dimensional interior acoustic problem with poroelastic materials. The system models an acoustic cavity measuring $1.122\,\mathrm{m} \times 0.82\,\mathrm{m} \times 0.982\,\mathrm{m}$ with two layers of different poroelastic materials covering one side. All walls surrounding the acoustic fluid are considered rigid and a sliding boundary condition is employed between the porous materials and the walls. The system is excited by an acoustic point source inside the cavity at the point $(1.03, 0.12, 0.30)$ and the sound pressure level L_p is evaluated at another location inside the cavity at $(0.35, 0.80, 0.10)$. A sketch of the system and its transfer function are given in fig. 6. The transfer function of this example is plotted over the frequency $f = \frac{\omega}{2\pi}$. Please note the peak in the transfer function near the zero frequency. This behavior can be observed in the numerical analysis of various acoustic settings and is caused by an internal mode of the acoustic fluid volume inside the cavity [59]. Detailed information about the geometry and material parameters for the poroelastic material are available in [60].

Each porous material consists out of an elastic skeleton which is filled by an acoustic fluid. The ratio between elastic and fluid phase is defined as the porosity ϕ and is the main characteristic of such materials. Their damping behavior is mainly caused by viscous and thermal effects of the fluid inside the pores and the structural damping of the elastic skeleton. This microscopic behavior is described by the Biot theory on a macroscopic level [7, 8] and has been adapted specifically for poro-acoustic systems by the Johnson-Champoux-Allard model [9, 26]. The dissipation mechanism is governed by

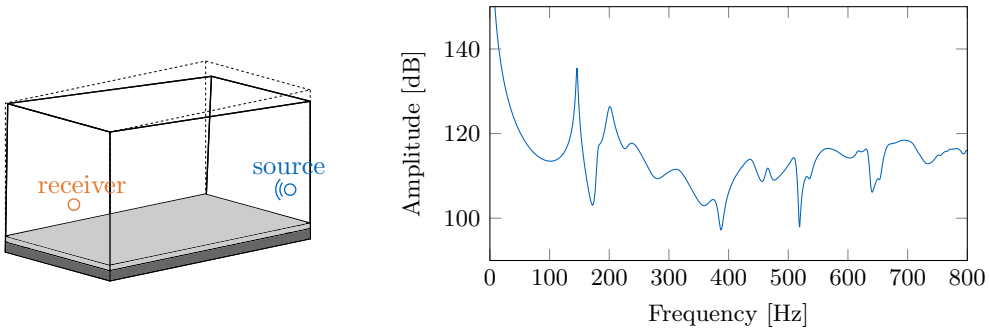

Figure 6: A sketch of the poro-acoustic system and the transfer function measuring the sound pressure level L_p at the receiver location. The dotted lines represent the maximum extents of the cavity in each axis ($1.122\,\mathrm{m} \times 0.82\,\mathrm{m} \times 0.982\,\mathrm{m}$), the solid lines show the actual walls of the box.

frequency-dependent, complex-valued functions for viscous drag $\tilde{b}(s)$ and effective bulk modulus of the fluid phase $\widetilde{K}_\mathrm{f}(s)$:

$$\tilde{b}(s) = \sigma\phi^2\sqrt{1 + \frac{4s\alpha_\infty^2\eta\rho_f}{\sigma^2\Lambda^2\phi^2}}, \tag{24}$$

$$\widetilde{K}_\mathrm{f}(s) = \frac{\gamma P_0}{\gamma - (\gamma-1)\left[1 + \frac{8\eta}{sPr\Lambda'^2\rho_\mathrm{f}}\sqrt{1 + \frac{sPr\Lambda'^2\rho_\mathrm{f}}{16\eta}}\right]^{-1}}. \tag{25}$$

Additionally to porosity ϕ and frequency s, they depend on the porous material's static flow resistivity σ, tortuosity α_∞, and viscous and thermal characteristic lengths Λ and Λ'. The interstitial fluid is described by its density ρ_f, viscosity η and heat capacity γ and is referenced to the standard pressure P_0. Pr is the Prandtl number. The parameters for eqs. (24) and (25) used in the numerical model are also given in [60]. Figure 7 plots the real and imaginary parts of the two parameters $\widetilde{K}_\mathrm{f}(s)$ and $\tilde{b}(s)$ for one of the considered poroelastic materials [60].

A finite element formulation using mixed degrees of freedom in the porous material, the so called $(\mathbf{u}, p)$ formulation, is used to discretize the problem [62]. Here, the fluid phase is described by its pressure p_f and the solid phase by its displacement vector $\mathbf{u}_\mathrm{s}$. Thus each node has four degrees of freedom in the 3d case. The acoustic pressure p_a inside the acoustic cavity is governed by the Helmholtz equation for a linear inviscid fluid. Off-diagonal coupling terms ensure the continuity between the poroelastic and acoustic domains and between the two poroelastic materials. After discretization with finite elements, the coupled system's transfer function is given by

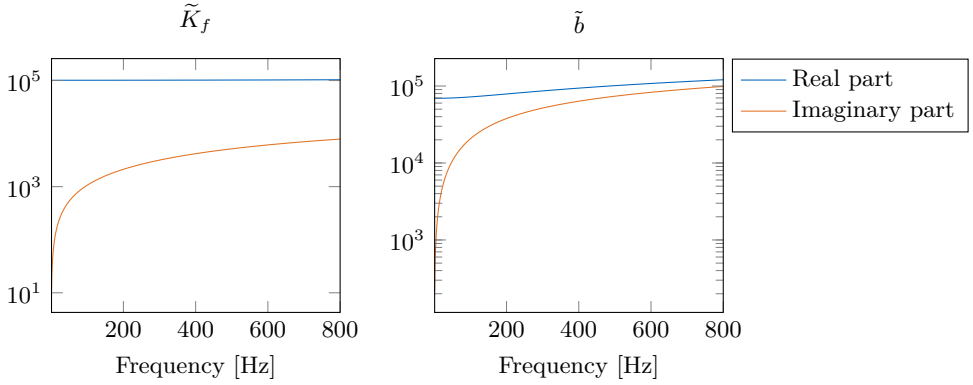

Figure 7: Real and imaginary parts of viscous drag $\tilde{b}$ and $\widetilde{K}_\mathrm{f}$ for a polyurethane foam with parameters $\phi = 0.93$, $\sigma = 80{\cdot}10^3\,\mathrm{kg\,m^{-3}\,s^{-1}}$, $\alpha_\infty = 2.5$, $\Lambda = 10{\cdot}10^{-6}\,\mathrm{m}$, $\Lambda' = 100{\cdot}10^{-6}\,\mathrm{m}$, $\rho_\mathrm{f} = 1.205\,\mathrm{kg\,m^{-3}}$, $\eta = 1.8208{\cdot}10^{-5}\,\mathrm{N\,s\,m^{-2}}$, $\gamma = 1.4$, $P_0 = 1.0128{\cdot}10^5\,\mathrm{Pa}$, $Pr = 0.712$ [60, 61].

$$
\begin{aligned}
H\left(s\right) = \mathbf{c}^\mathsf{T} \Bigg(& \mathbf{A}_{0,p_1} - \tilde{\gamma}_{p_1}\mathbf{G}_{1,p_1} - \frac{\phi_{p_1}^2}{\widetilde{R}_{p_1}}\mathbf{G}_{2,p_1} - \frac{\phi_{p_1}^2}{s^2\tilde{\rho}_{22,p_1}}\mathbf{G}_{3,p_1} + s^2\tilde{\rho}_{p_1}^*\mathbf{G}_{4,p_1} - \xi_{p_1}\mathbf{G}_{5,p_1} \\
& + \mathbf{A}_{0,p_2} - \tilde{\gamma}_{p_2}\mathbf{G}_{1,p_2} - \frac{\phi_{p_2}^2}{\widetilde{R}_{p_2}}\mathbf{G}_{2,p_2} - \frac{\phi_{p_2}^2}{s^2\tilde{\rho}_{22,p_2}}\mathbf{G}_{3,p_2} + s^2\tilde{\rho}_{p_2}^*\mathbf{G}_{4,p_2} \\
& + \mathbf{A}_{0,a} - \frac{1}{s^2}\mathbf{G}_{1,a}\Bigg)^{-1}\mathbf{b}, \qquad (26)
\end{aligned}
$$

where the indices p_1 and p_2 identify the matrices and functions associated with the two porous materials and index a marks the quantities associated with the acoustic cavity. The factors $\tilde{\gamma}$, $\widetilde{R}$, $\tilde{\rho}_{22}$, and $\tilde{\rho}^*$ contain viscous drag $\tilde{b}$ and effective bulk modulus $\widetilde{K}_\mathrm{f}$ of the respective porous material; they are given, for example, in [9]. The coupling between the poroelastic and acoustic domains is given by $\xi_{p_1} = \frac{(1-\phi)^2}{\phi}\widetilde{K}_{\mathrm{f},p_1}$ and leads to non-symmetric matrices due to off-diagonal coupling terms. Thus, the discretized system contains ten frequency dependent functions: four for each poroelastic material, one for the acoustic cavity, and one for the coupling of poroelastic material and acoustic fluid. Given a tolerance of $1{\cdot}10^{-14}$, AAA computes rational approximations of all involved frequency-dependent functions with orders of 40 or less. The numerical model considered in the experiments is of size $n = 56\,374$ and is evaluated in the frequency range from 1 to 800 Hz. The evaluation of the full model in steps of 1 Hz took $t_\mathrm{c} \approx 5.6{\cdot}10^4\,\mathrm{s} \approx 15.6\,\mathrm{h}$.

4.2.1. Influence of the expansion error on the reduced order model

The influence of the approximation of the matrix inverse in eq. (17) by a Neumann series expansion is examined in the following. This approximation can become unstable for s far away from the shift s_0. However, the approximation error of the reduced model can still be acceptable in these regions, as it is shown in fig. 8. Here, reduced models

shifted about $s_0 = 2\pi\mathrm{i} \cdot 400$ with $r = 400$ and different Krylov subspace orders k are compared. Additionally, the highest approximation error of the Neumann series compared to the respective original function is given for each k. The function with the highest error is chosen from the ten frequency dependent functions considered in the model. It can be seen, that increasing the subspace order k also widens the frequency range around the chosen shift, where the reduced model is accurate (solid lines in fig. 8). Accordingly, the accuracy of the series expansion increases with increasing order k (dashed lines in fig. 8). This expansion has very high relative errors for low frequencies, which does not impair the approximation quality of the reduced model, as the influence of the function is apparently low in this frequency region. However, an approximation based on an expansion point located in this frequency region might have a large influence on the approximation quality of the reduced model in the higher frequency region. As this is problem dependent, the employed series expansions should be examined prior to the reduction process in order to avoid placing expansion points in such regions. Note, that the relative error ε_e considering the expanded approximation and the original function is identical to the error of a Taylor series expansion with same shift and order.

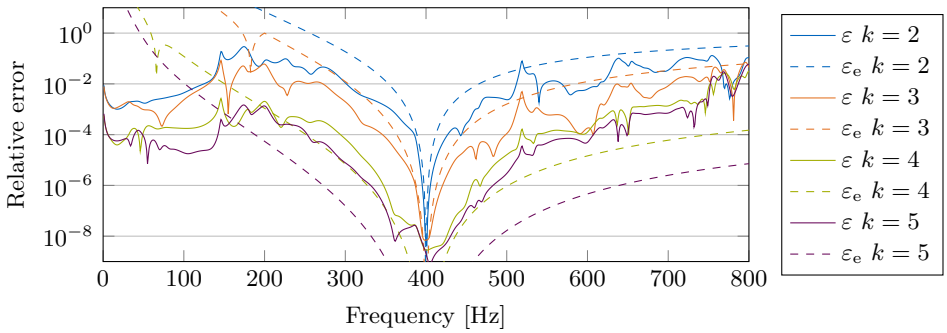

Figure 8: Reduction errors ε for different k and the Neumann expansion error ε_e for the respective function with the highest error regarding the poroacoustic model. The reduced models are expanded about $s_0 = 2\pi\mathrm{i} \cdot 400$ with $r = 400$.

We found that especially the polynomial expansions of the functions associated to $\mathbf{G}_{3,p_1}$ and $\mathbf{G}_{3,p_2}$ in eq. (26) are prone to instabilities if an expansion point in the low frequency region is chosen. Multiplying all terms in eq. (26) by s^2 cancels out $1/s^2$ terms in the corresponding frequency-dependent functions, which was found to increase the approximation quality of the reduced order models in most of the considered frequency range. This behavior is shown in fig. 9 and this modified formulation is used in the following numerical experiments. Again, this is problem dependent and a thorough investigation of the behavior of the Neumann expansion before the reduction process can be beneficial.

4.2.2. Influence of subspace order k on the accuracy

We now investigate the influence of the Krylov subspace order k on the approximation quality of reduced order models with different sizes r. The models are computed using reduction bases with a single expansion point at $s_0 = 2\pi\mathrm{i} \cdot 400$. The approximate relative

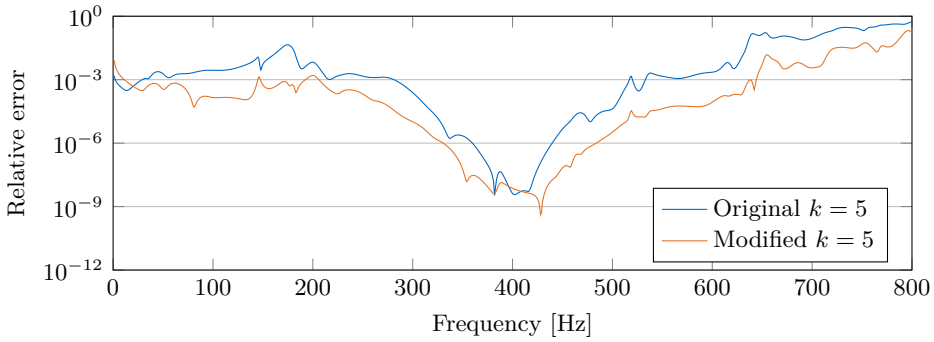

Figure 9: Approximation error of the original and modified poroacoustic models. A single Krylov subspace of order $k = 5$ with expansion point $s_0 = 2\pi\mathrm{i} \cdot 400$ is considered. The reduced model has an order of $r = 200$.

$\mathcal{L}_\infty$-errors in the frequency range $f = [1, \ldots, 800]$ for all combinations of r and k are given in fig. 10. It can be seen, that a higher order k leads to more accurate reduced models if the reduced order r is kept constant. The error of the models based on subspaces with $k = 2$ is nearly a magnitude higher than the other reduced models', especially for higher reduced orders r. This suggests that by truncating after the quadratic terms of the AAA approximation, important parts of the frequency-dependent functions are neglected. However, the effect of further increasing the subspace order has a smaller effect in terms of accuracy, suggesting that all functions are sufficiently approximated for $k > 3$.

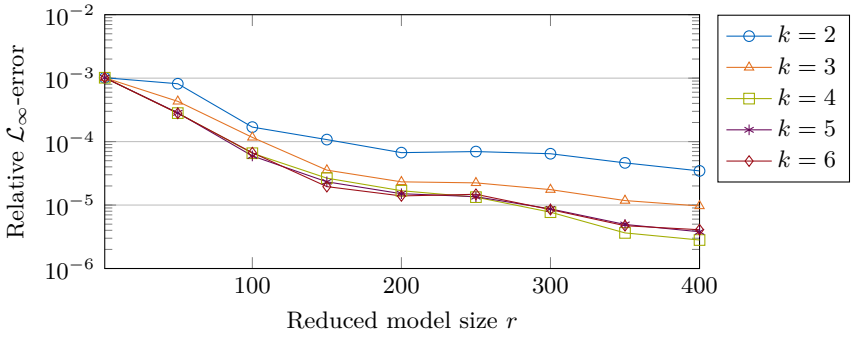

Figure 10: Relative errors in the frequency range $f = [1, \ldots, 800]$ of reduced models of different sizes r and Krylov subspace orders k. All subspaces are expanded around $s_0 = 2\pi\mathrm{i} \cdot 400$.

The better accuracy of the higher-order Krylov subspace comes with increased computational cost. Figure 11 plots the required computation times for the same models as above with increasing r against their approximate relative $\mathcal{L}_\infty$-errors. The curves begin at $r = 1$ at their leftmost points, while the rightmost data points correspond to $r = 400$. While increasing k leads to lower maximum errors, the computation time is

also increased. It can be seen, that using lower orders of k in combination with a higher reduced order r has the potential to yield as accurate reduced order models in the same time as employing a higher k in combination with a lower r. In this example, the reduced order r is the limiting factor regarding accuracy, as it has a larger influence on the transfer function of the reduced models than the accurate representation of the frequency dependent functions. The results suggest, that the benefit of higher orders k is small if the computation times are crucial for the application. However, the computation times for all models are still much lower than the time required for the evaluation of the full model.

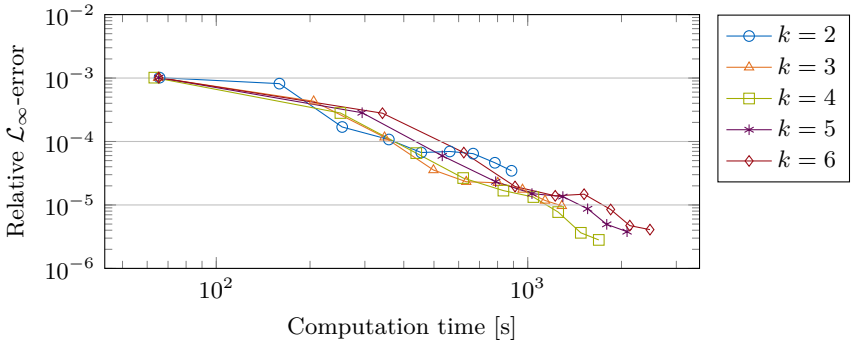

Figure 11: Relative errors in the frequency range $f = [1, \ldots, 800]$ of reduced models of different sizes r and Krylov subspace orders k over the required computation time. All models are computed using a single expansion point $s_0 = 2\pi\mathrm{i} \cdot 400$. The curves begin at $r = 1$ at their leftmost points, while the rightmost data point corresponds to $r = 400$.

4.2.3. Multi-point moment matching

In order to obtain a reduced order model of reasonable size with high accuracy over a wide frequency range, multiple Krylov spaces can be combined to a single projection basis. We again consider different orders k of the employed Krylov spaces while their size r remains constant. We start with a model computed from four expansion points $s_{0,i} = 2\pi\mathrm{i}\,[100, 300, 500, 700]$ distributed linearly in the frequency range of interest. An order $r_0 = 100$ is considered for each subspace, thus the resulting reduced model has an order of $r = 400$. Their relative errors are given in fig. 12. Again, the influence of higher orders k can be observed in an increased accuracy between the expansion points. Comparing the relative errors to the reduced models computed from a single expansion point reported in fig. 8, the benefit of multiple expansion points is obvious. Despite having the same reduced order, the relative error is lower for a wider frequency range if more than one expansion point is chosen. An uninformed a priori choice of expansion point locations and reduced order may, however, not be ideal and result in too large or inaccurate reduced models.

4.3. Adaptive model order reduction

Therefore, the adaptive procedure given in algorithm 3.1 is now used to compute reduced models of the poroacoustic system. The reduced order models should be valid

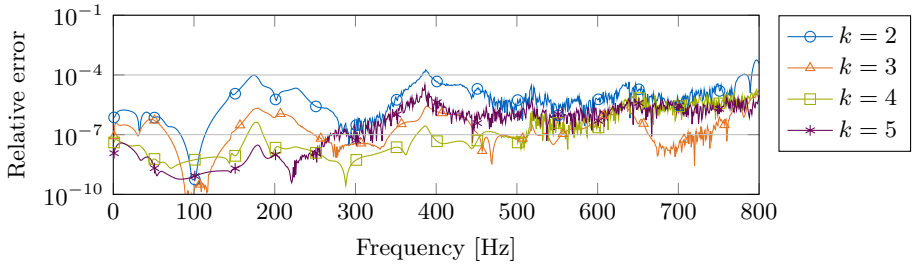

Figure 12: Approximation error of reduced order models approximating the poroacoustic system. Approximation with different orders k of the Krylov spaces around $s_{0,i} = 2\pi\mathrm{i}\,[100, 300, 500, 700]$ with reduced orders $r_0 = 100$ each. The resulting model is of order $r = 400$.

in the frequency range $f = [1, \ldots, 800]$. As algorithm 3.1 allows variation in the input parameters, different starting conditions are considered for the numerical experiments:

- Experiment A: Varying $k_{\min} = [2, 3, 4]$, fixed $k_{\max} = 6$ and $k_{\text{incr}} = 1$,
- Experiment B: Varying $k_{\min} = [2, 3, 4]$, fixed $k_{\text{incr}} = 1$, setting $k_{\max} = k_{\min} + k_{\text{incr}}$,
- Experiment C: Varying $k_{\min} = [2, 3]$, setting $k_{\text{incr}} = k_{\min}$ and $k_{\max} = k_{\min} + k_{\text{incr}}$.

$k_{\max} = 6$ was chosen for all experiments because the expansion factors obtained from eq. (18) are close to zero for higher orders. The local subspace size $r_{0,i}, i = 1, \ldots, n_{\text{s}}$ is set to 50 for all experiments. The algorithm stops, if an error smaller than $\varepsilon_{\text{tol}} = 1{\cdot}10^{-5}$ is estimated or the reduced model reaches the maximum order of $r_{\max} = 1000$. Each experiment is performed with a varying number of initial expansion points $n_{\text{s}} = [1, \ldots, 6]$ distributed linearly in the range $s = 2\pi\mathrm{i}\,[100, \ldots, 800]$. Expansion points corresponding to lower frequencies are not considered in this example, as they would excite the unstable pole near the zero frequency [59] and resulting reduced order models might also exhibit this instability. Additionally, the expanded frequency-dependent functions tend to be unstable if an expansion point in the low frequency range is chosen, as reported in section 4.2.1. For each n_{s} a reference solution obtained from using standard second-order Krylov subspaces is computed. This solution is also obtained from algorithm 3.1 by setting $k_{\min} = k_{\max} = 2$, such that the same error estimation process and greedy choice of new expansion points is performed during all experiments. The resulting computation times and sizes of the reduced order models are reported in graphical form and grouped by the considered $k_{\min}$ in figs. 13 to 15. Here, the reduced order r encodes the number of considered expansion points at convergence by $n_{\text{s,conv}} = r/50$, as the algorithm does not increase the size of the individual Krylov spaces. Tables 1 and 2 present these results in tabular form, the approximation errors of the obtained reduced order models are also given there.

Most numerical experiments resulted in reduced order models having a maximum error lower than or comparable to the defined threshold $\varepsilon_{\text{tol}} = 1{\cdot}10^{-5}$ and all initial configurations converged before the reduced order model reached the maximum size of $r_{\max} = 1000$. Comparing the adaptive algorithm with variable k to the reference employing a second-order Krylov subspace shows that using a variable k yields smaller reduced

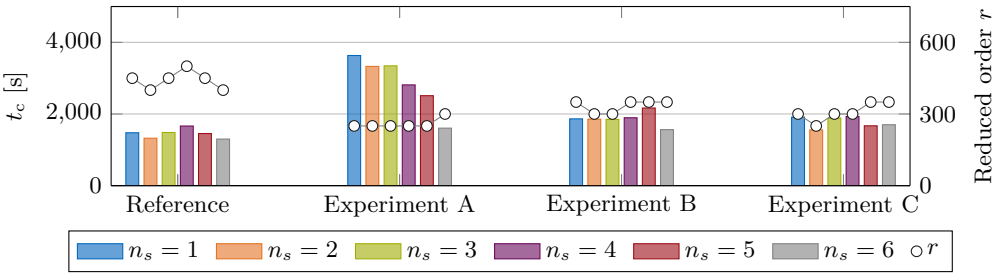

Figure 13: Comparison of the computation times t_c (bars) and resulting reduced orders r (circles) for experiments with $k_{\min} = 2$ to the reference second-order Krylov space.

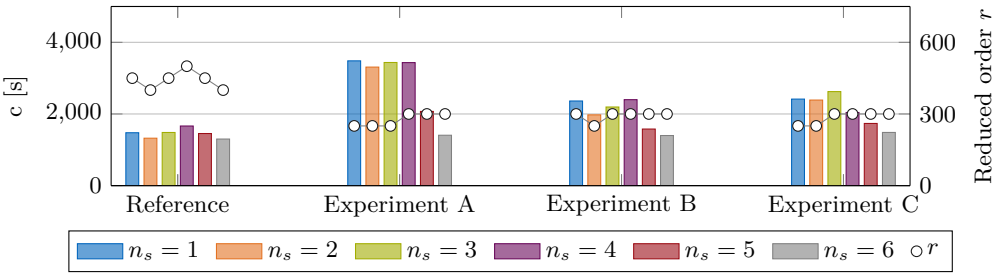

Figure 14: Comparison of the computation times t_c (bars) and resulting reduced orders r (circles) for experiments with $k_{\min} = 3$ to the reference second-order Krylov space.

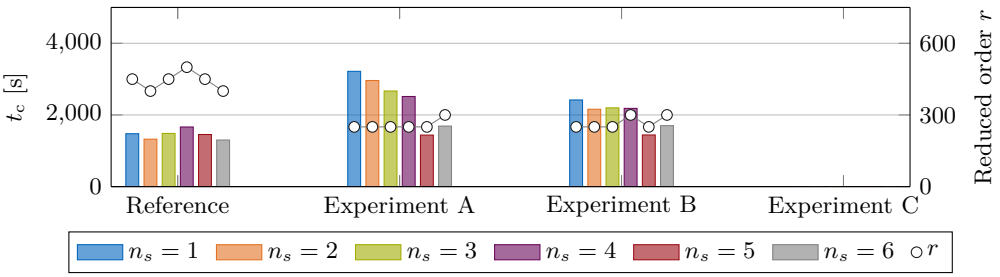

Figure 15: Comparison of the computation times t_c (bars) and resulting reduced orders r (circles) for experiments with $k_{\min} = 4$ to the reference second-order Krylov space.

order models at the cost of longer computation times. Especially Experiment A has considerably longer computation times than the reference solution, while the algorithm often finishes in comparable time to the reference case given the settings of Experiments B and C. The longer computation times for Experiment A can be explained by the fact that for increasing k at a specific shift, no previous results can be reused. Incrementing k a few times before reaching $k_{\max}$ as in Experiment A thus involves some redundant computations.

The reduced order models obtained from all experiments are considerably smaller than the ones computed by the reference experiment. The reduced order models obtained from Experiment A tend to be the smallest, their size is mostly not affected by the number of

Table 1: Detailed results of the adaptive algorithm applied to the poroacoustic model regarding the three initial configurations with $n_\mathrm{s} = [1, 2, 3]$ for the reference solution and the three experiments A, B, and C. Given are the order of the reduced order model, the maximum relative approximation error in the frequency range of interest, and the computation time t_c.

n_s	Exp.	k_min	k_max	k_incr	r	$n_\mathrm{s,conv}$	$\max \varepsilon$	t_c[s]	t_c[min]
1	Ref.				450	9	$4.01{\cdot}10^{-6}$	1476.0	24.6
	A	2	6	1	250	5	$1.86{\cdot}10^{-6}$	3632.3	60.5
		3	6	1	250	5	$1.02{\cdot}10^{-6}$	3482.6	58.0
		4	6	1	250	5	$1.96{\cdot}10^{-6}$	3217.8	53.6
	B	2	3	1	350	7	$6.16{\cdot}10^{-6}$	1864.0	31.1
		3	4	1	300	6	$1.46{\cdot}10^{-6}$	2362.1	39.4
		4	5	1	250	5	$1.83{\cdot}10^{-6}$	2418.3	40.3
	C	2	4	2	300	6	$9.04{\cdot}10^{-7}$	1912.2	31.9
		3	6	3	250	5	$1.29{\cdot}10^{-6}$	2415.2	40.3
2	Ref.				400	8	$5.57{\cdot}10^{-6}$	1323.8	22.1
	A	2	6	1	250	5	$1.91{\cdot}10^{-6}$	3328.5	55.5
		3	6	1	250	5	$2.40{\cdot}10^{-6}$	3308.4	55.1
		4	6	1	250	5	$1.43{\cdot}10^{-6}$	2961.1	49.4
	B	2	3	1	300	6	$6.24{\cdot}10^{-6}$	1855.5	30.9
		3	4	1	250	5	$5.01{\cdot}10^{-6}$	1974.9	32.9
		4	5	1	250	5	$5.67{\cdot}10^{-6}$	2159.6	36.0
	C	2	4	2	250	5	$7.07{\cdot}10^{-6}$	1554.6	25.9
		3	6	3	250	5	$2.61{\cdot}10^{-6}$	2388.4	39.8
3	Ref.				450	9	$4.22{\cdot}10^{-6}$	1483.4	24.7
	A	2	6	1	250	5	$2.27{\cdot}10^{-6}$	3344.1	55.7
		3	6	1	250	5	$1.07{\cdot}10^{-6}$	3436.8	57.3
		4	6	1	250	5	$1.49{\cdot}10^{-6}$	2668.7	44.5
	B	2	3	1	300	6	$4.36{\cdot}10^{-6}$	1847.9	30.8
		3	4	1	300	6	$2.04{\cdot}10^{-6}$	2194.5	36.6
		4	5	1	250	5	$2.22{\cdot}10^{-6}$	2198.3	36.6
	C	2	4	2	300	6	$9.52{\cdot}10^{-7}$	1887.8	31.5
		3	6	3	300	6	$5.45{\cdot}10^{-7}$	2624.6	43.7

n_s. The sizes of the reduced order models obtained from Experiments B and C also do not differ much. No benefit regarding size or computation time can be observed by choosing a higher increment k_incr in Experiment C as compared to $k_\mathrm{incr} = 1$ in Experiment B.

Increasing the number of initial expansion points n_s shows a tendency for decreasing computation times, especially for Experiment A. For $n_\mathrm{s} = 5$ and $n_\mathrm{s} = 6$ some experiments with settings A and B converged without establishing an additional expansion point. In the reference experiments at least two additional expansion points, each of local order $r_0 = 50$, are required to obtain a reduced order model of comparable accuracy for $n_\mathrm{s} = 6$. The smaller size of the reduced order models computed from Experiments A and B with

Table 2: Detailed results of the adaptive algorithm applied to the poroacoustic model regarding the three initial configurations with $n_\mathrm{s} = [4, 5, 6]$ for the reference solution and the three experiments A, B, and C. Given are the order of the reduced order model, the maximum relative approximation error in the frequency range of interest, and the computation time t_c.

n_s	Exp.	k_min	k_max	k_incr	r	$n_\mathrm{s,conv}$	$\max \varepsilon$	t_c[s]	t_c[min]
4	Ref.				500	10	$3.68{\cdot}10^{-7}$	1664.0	27.7
	A	2	6	1	250	5	$3.10{\cdot}10^{-5}$	2812.2	46.9
		3	6	1	300	6	$5.65{\cdot}10^{-7}$	3433.3	57.2
		4	6	1	250	5	$2.62{\cdot}10^{-5}$	2515.2	41.9
	B	2	3	1	350	7	$1.51{\cdot}10^{-6}$	1894.7	31.6
		3	4	1	300	6	$2.00{\cdot}10^{-6}$	2399.0	40.0
		4	5	1	300	6	$1.53{\cdot}10^{-6}$	2183.2	36.4
	C	2	4	2	300	6	$6.94{\cdot}10^{-7}$	1928.4	32.1
		3	6	3	300	6	$2.27{\cdot}10^{-6}$	2041.6	34.0
5	Ref.				450	9	$5.35{\cdot}10^{-6}$	1454.2	24.2
	A	2	6	1	250	5	$4.82{\cdot}10^{-6}$	2510.7	41.8
		3	6	1	300	6	$1.25{\cdot}10^{-5}$	2071.2	34.5
		4	6	1	250	5	$1.42{\cdot}10^{-6}$	1437.9	24.0
	B	2	3	1	350	7	$1.38{\cdot}10^{-6}$	2166.7	36.1
		3	4	1	300	6	$1.32{\cdot}10^{-5}$	1579.3	26.3
		4	5	1	250	5	$1.42{\cdot}10^{-6}$	1441.6	24.0
	C	2	4	2	350	7	$9.05{\cdot}10^{-6}$	1670.4	27.8
		3	6	3	300	6	$1.58{\cdot}10^{-5}$	1735.4	28.9
6	Ref.				400	8	$2.77{\cdot}10^{-6}$	1300.2	21.7
	A	2	6	1	300	6	$5.76{\cdot}10^{-6}$	1605.2	26.8
		3	6	1	300	6	$2.06{\cdot}10^{-6}$	1406.4	23.4
		4	6	1	300	6	$2.00{\cdot}10^{-6}$	1689.4	28.2
	B	2	3	1	350	7	$3.07{\cdot}10^{-6}$	1563.2	26.1
		3	4	1	300	6	$2.06{\cdot}10^{-6}$	1398.4	23.3
		4	5	1	300	6	$2.00{\cdot}10^{-6}$	1700.8	28.3
	C	2	4	2	350	7	$3.48{\cdot}10^{-6}$	1700.0	28.3
		3	6	3	300	6	$1.48{\cdot}10^{-6}$	1484.5	24.7

computation times comparable to the reference case shows a benefit of employing higher-order Krylov subspaces.

The computation times and reduced order model sizes observed in all three experiments are not heavily influenced by the initial Krylov subspace order k_min, although the computation times tend to be a bit shorter with increasing k_min. Increasing the Krylov subspace order by more than $k_\mathrm{incr} = 1$ seems not to be beneficial, shown by the very similar results of Experiments B and C. However, this shows the robustness of the workflow regarding a perhaps not always optimal choice of the parameters k_min and k_incr.

Starting with fewer expansion points typically requires longer computation times in

order to obtain accurate reduced order models when incrementing the Krylov subspace order by $k_{\text{incr}} = 1$ to $k_{\max} = 6$ in Experiment A. However, the reduced models are small compared to the reference case. This investment in longer computation time can be reasonable, if, for example, the goal of the reduction process is a model being as small as possible. Experiments B and C show nearly the same computation times for all configurations of initial expansion points. The fact that accurate reduced order models can be obtained from one initial expansion point for the reference case as well as all experiments considering higher-order Krylov subspaces shows the robustness of the error estimation and the greedy approach.

5. Conclusions

We have presented a workflow to reduce the numerical complexity of dynamic systems with frequency-dependent material properties. Additionally, we have presented an adaptive algorithm to automatically compute such reduced models with a defined accuracy requiring as little a priori information as possible about the original system. The employed reduction framework automatically converts the original transfer function containing frequency-dependent functions to a purely polynomial transfer function, which can be employed in a moment matching method afterwards. This conversion is performed automatically and is not limited to specific types of functions. Using a higher-order Krylov space for moment matching allows to consider also higher-order polynomials and potentially yields smaller reduced models compared to a low-order Krylov space, while reaching a similar accuracy. This, however, requires more computational resources and if the runtime of the reduction process is crucial, a standard second-order Krylov space may be sufficient. If the reduced order model should be as small as possible, a higher-order Krylov space may be beneficial.

In order to compute reasonably-sized reduced order models of systems with frequency-dependent damping effects, we have presented an adaptive algorithm. Its only input parameters are the frequency range in which the reduced model should approximate the original system and a tolerance. It automatically chooses a reasonable Krylov subspace order and only increases the size of the reduced order model if necessary. The resulting reduced order models are usually smaller than the models obtained employing only second-order Krylov spaces. The employed error estimator is prone to slightly underestimate the exact approximation error, but the reduced models are mostly as accurate as required. In order to reduce the computation time of the adaptive algorithm, it would be beneficial to modify the higher-order Arnoldi algorithm such that it can be restarted at a previously computed order k.

The reduction framework can be applied to any system whose transfer function contains nonlinear functions depending on the excitation frequency. The method's performance should be evaluated by applying it to more types of systems with frequency dependent functions. One example also from the vibro-acoustic context would be the application of radiating boundary conditions. A perfectly matched layer (PML), for example, can be formulated as a dissipative material with frequency dependent properties. As systems modeling radiation problems are typically very large, a complexity reduction is beneficial here [63, 64].

Acknowledgments

Some of the numerical experiments have been conducted while Q. Aumann was at the Max Planck Institute for Dynamics of Complex Technical Systems in Magdeburg, Germany. The computational and data resources provided by the Max Planck Institute Magdeburg are gratefully acknowledged.

The research of S. Jonckheere is funded by a grant from the Flanders Innovation & Entrepreneurship Agency. Internal Funds KU Leuven are gratefully acknowledged for their support.

References

[1] S. Marburg, Developments in structural-acoustic optimization for passive noise control, Arch. Computat. Methods Eng. 9 (4) (2002) 291–370. doi:10.1007/BF03041465.

[2] F. Duddeck, Multidisciplinary optimization of car bodies, Struct. Multidiscip. O. 35 (4) (2008) 375–389. doi:10.1007/s00158-007-0130-6.

[3] C. C. Claeys, K. Vergote, P. Sas, W. Desmet, On the potential of tuned resonators to obtain low-frequency vibrational stop bands in periodic panels, J. Sound Vib. 332 (6) (2013) 1418–1436. doi:10.1016/j.jsv.2012.09.047.

[4] S. J. Elliott, M. Ghandchi Tehrani, R. S. Langley, Nonlinear damping and quasi-linear modelling, Philos. T. Roy. Soc. A 373 (2051). doi:10.1098/rsta.2014.0402.

[5] K. Amichi, N. Atalla, A New 3D Finite Element for Sandwich Beams With a Viscoelastic Core, J. Vib. Acoust. 131 (2). doi:10.1115/1.3025828.

[6] R. van Beeumen, K. Meerbergen, W. Michiels, A Rational Krylov Method Based on Hermite Interpolation for Nonlinear Eigenvalue Problems, SIAM J. Sci. Comput. 35 (1) (2013) A327–A350. doi:10.1137/120877556.

[7] M. A. Biot, Theory of Propagation of Elastic Waves in a Fluid-Saturated Porous Solid. I. Low-Frequency Range, J. Acoust. Soc. Am. 28 (2) (1956) 168–178. doi:10.1121/1.1908239.

[8] M. A. Biot, Theory of Propagation of Elastic Waves in a Fluid-Saturated Porous Solid. II. Higher Frequency Range, J. Acoust. Soc. Am. 28 (2) (1956) 179–191. doi:10.1121/1.1908241.

[9] J.-F. Allard, N. Atalla, Propagation of sound in porous media: Modelling sound absorbing materials, 2nd Edition, Wiley, Hoboken, NJ, 2009. doi:10.1002/9780470747339.

[10] R. Rumpler, Efficient finite element approach for structural-acoustic applications including 3D modelling of sound absorbing porous materials, Vol. 2012:10 of TRITA-AVE, Engineering Sciences, Royal Institute of Technology, Stockholm, 2012.

[11] A. C. Antoulas, C. A. Beattie, S. Gugercin, Interpolatory methods for model reduction, Vol. 21 of Computational science and engineering, Society for Industrial and Applied Mathematics, Philadelphia, 2020. doi:10.1137/1.9781611976083.

[12] U. Hetmaniuk, R. Tezaur, C. Farhat, Review and assessment of interpolatory model order reduction methods for frequency response structural dynamics and acoustics problems, Int. J. Numer. Meth. Engng. 90 (13) (2012) 1636–1662. doi:10.1002/nme.4271.

[13] S. van Ophem, O. Atak, E. Deckers, W. Desmet, Stable model order reduction for time-domain exterior vibro-acoustic finite element simulations, Comput. Methods Appl. Mech. Eng. 325 (2017) 240–264. doi:10.1016/j.cma.2017.06.022.

[14] L. Rouleau, J.-F. Deü, A. Legay, A comparison of model reduction techniques based on modal projection for structures with frequency-dependent damping, Mech. Syst. Signal Pr. 90 (2017) 110–125. doi:10.1016/j.ymssp.2016.12.013.

[15] S. M. Kim, J.-G. Kim, S.-W. Chae, K. C. Park, A strongly coupled model reduction of vibro-acoustic interaction, Comput. Methods Appl. Mech. Eng. 347 (2019) 495–516. doi:10.1016/j.cma.2018.12.029.

[16] E. Deckers, W. Desmet, K. Meerbergen, F. Naets, Case studies of model order reduction for acoustics and vibrations, in: P. Benner, S. Grivet-Talocia, A. Quarteroni, G. Rozza, W. Schilders, L. M. Silveira (Eds.), Model order reduction – Volume 3: Applications, De Gruyter, 2021, pp. 76–110. doi:10.1515/9783110499001-003.

[17] C. Beattie, S. Gugercin, Interpolatory projection methods for structure-preserving model reduction, Syst. Control Lett. 58 (3) (2009) 225–232. doi:10.1016/j.sysconle.2008.10.016.

[18] C. Beattie, S. Gugercin, Realization-independent H2-approximation, in: 2012 IEEE 51st IEEE Conference on Decision and Control (CDC), IEEE, 2012, pp. 4953–4958. doi:10.1109/CDC.2012.6426344.

[19] K. Sinani, S. Gugercin, C. Beattie, A Structure-preserving Model Reduction Algorithm for Dynamical Systems with Nonlinear Frequency Dependence, IFAC-PapersOnLine 49 (9) (2016) 56–61. doi:10.1016/j.ifacol.2016.07.492.

[20] A. J. Mayo, A. C. Antoulas, A framework for the solution of the generalized realization problem, Linear Algebra Appl. 425 (2-3) (2007) 634–662. doi:10.1016/j.laa.2007.03.008.

[21] A. A. Phoenix, P. A. Tarazaga, Dynamic model reduction using data-driven Loewner-framework applied to thermally morphing structures, Journal of Sound and Vibration 396 (2017) 274–288. doi:10.1016/j.jsv.2017.01.039.

[22] B. Peherstorfer, K. Willcox, Data-driven operator inference for nonintrusive projection-based model reduction, Computer Methods in Applied Mechanics and Engineering 306 (2016) 196–215. doi:10.1016/j.cma.2016.03.025.

[23] P. Benner, P. Goyal, B. Kramer, B. Peherstorfer, K. Willcox, Operator inference for non-intrusive model reduction of systems with non-polynomial nonlinear terms, Comput. Methods Appl. Mech. Eng. 372 (2020) 113433. doi:10.1016/j.cma.2020.113433.

[24] Y. C. Liang, H. P. Lee, S. P. Lim, W. Z. Lin, K. H. Lee, C. G. Wu, Proper Orthogonal Decomposition and its Applications—Part I: Theory, Journal of Sound and Vibration 252 (3) (2002) 527–544. doi:10.1006/jsvi.2001.4041.

[25] J. H. Tu, C. W. Rowley, D. M. Luchtenburg, S. L. Brunton, N. J. Kutz, On dynamic mode decomposition: Theory and applications, Journal of Computational Dynamics 1 (2) (2014) 391–421. doi:10.3934/jcd.2014.1.391.

[26] R. Rumpler, P. Göransson, J.-F. Deü, A finite element approach combining a reduced-order system, Padé approximants, and an adaptive frequency windowing for fast multi-frequency solution of poro-acoustic problems, Int. J. Numer. Meth. Engng. 97 (10) (2014) 759–784. doi:10.1002/nme.4609.

[27] R. Rumpler, Padé approximants and the modal connection: Towards increased robustness for fast parametric sweeps, Int. J. Numer. Meth. Engng. 113 (1) (2018) 65–81. doi:10.1002/nme.5603.

[28] P. Lietaert, J. Pérez, B. Vandereycken, K. Meerbergen, Automatic rational approximation and linearization of nonlinear eigenvalue problems.
URL http://arxiv.org/pdf/1801.08622v2

[29] Y. Nakatsukasa, O. Sète, L. N. Trefethen, The AAA Algorithm for Rational Approximation, SIAM J. Sci. Comput. 40 (3) (2018) A1494–A1522. doi:10.1137/16M1106122.

[30] Z. Bai, Y. Su, Dimension Reduction of Large-Scale Second-Order Dynamical Systems via a Second-Order Arnoldi Method, SIAM J. Sci. Comput. 26 (5) (2005) 1692–1709. doi:10.1137/040605552.

[31] D. Lu, Y. Su, Z. Bai, Stability Analysis of the Two-level Orthogonal Arnoldi Procedure, SIAM J. Matrix Anal. & Appl. 37 (1) (2016) 195–214. doi:10.1137/151005142.

[32] X. Xie, H. Zheng, S. Jonckheere, A. van de Walle, B. Pluymers, W. Desmet, Adaptive model reduction technique for large-scale dynamical systems with frequency-dependent damping, Comput. Methods Appl. Mech. Eng. 332 (2018) 363–381. doi:10.1016/j.cma.2017.12.023.

[33] Y. Lin, L. Bao, Y. Wei, Model-order reduction of large-scale kth-order linear dynamical systems via a kth-order Arnoldi method, Int. J. Comput. Math. 87 (2) (2010) 435–453. doi:10.1080/00207160802130164.

[34] U. Hetmaniuk, R. Tezaur, C. Farhat, An adaptive scheme for a class of interpolatory model reduction methods for frequency response problems, Int. J. Numer. Meth. Engng. 93 (10) (2013) 1109–1124. doi:10.1002/nme.4436.

[35] A. Bodendiek, M. Bollhöfer, Adaptive-order rational Arnoldi-type methods in computational electromagnetism, BIT Numer. Math. 54 (2) (2014) 357–380. doi:10.1007/s10543-013-0458-9.

[36] L. Feng, J. G. Korvink, P. Benner, A Fully Adaptive Scheme for Model Order Reduction Based on Moment Matching, IEEE Trans. Compon., Packag. Manufact. Technol. 5 (12) (2015) 1872–1884. doi:10.1109/TCPMT.2015.2491341.

[37] Q. Aumann, G. Müller, Robust error assessment for reduced order vibro-acoustic problems, in: Proceedings of ISMA 2020, KU Leuven - Department of Mechanical Engineering, 2020, pp. 1901–1914.

[38] J. Fehr, P. Eberhard, Error-Controlled Model Reduction in Flexible Multibody Dynamics, J. Comput. Nonlinear Dynam. 5 (3). doi:10.1115/1.4001372.

[39] T. Bonin, H. Faßbender, A. Soppa, M. Zaeh, A fully adaptive rational global Arnoldi method for the model-order reduction of second-order MIMO systems with proportional damping, Math. Comput. Simulat. 122 (2016) 1–19. doi:10.1016/j.matcom.2015.08.017.

[40] G. Rozza, D. B. P. Huynh, A. T. Patera, Reduced basis approximation and a posteriori error estimation for affinely parametrized elliptic coercive partial differential equations, Archives of Computational Methods in Engineering 15 (3) (2008) 229–275. doi:10.1007/s11831-008-9019-9.
[41] A. Quarteroni, A. Manzoni, F. Negri, Reduced Basis Methods for Partial Differential Equations, Springer International Publishing, 2016. doi:10.1007/978-3-319-15431-2.
[42] S. K. Baydoun, M. Voigt, C. Jelich, S. Marburg, A greedy reduced basis scheme for multi-frequency solution of structural acoustic systems, International Journal for Numerical Methods in Engineeringdoi:10.1002/nme.6205.
[43] E. J. Grimme, Krylov Projection Methods for Model Reduction, Dissertation, University of Illinois at Urbana-Champaign (1997).
URL http://hdl.handle.net/2142/81180
[44] L. Feng, A. C. Antoulas, P. Benner, Some a posteriori error bounds for reduced-order modelling of (non-)parametrized linear systems, ESAIM: M2AN 51 (6) (2017) 2127–2158. doi:10.1051/m2an/2017014.
[45] L. Feng, P. Benner, On Error Estimation for Reduced-order Modeling of Linear Non-parametric and Parametric Systems.
URL http://arxiv.org/pdf/2003.14319v2
[46] J. Jith, S. Sarkar, A model order reduction technique for systems with nonlinear frequency dependent damping, Appl. Math. Model. 77 (2020) 1662–1678. doi:10.1016/j.apm.2019.08.030.
[47] X. Xie, H. Zheng, S. Jonckheere, W. Desmet, Acoustic simulation of cavities with porous materials using an adaptive model order reduction technique, J. Sound Vib. 485 (2020) 115570. doi:10.1016/j.jsv.2020.115570.
[48] S. A. Wyatt, Issues in Interpolatory Model Reduction: Inexact Solves, Second-order Systems and DAEs, Dissertation, Virginia Polytechnic Institute and State University (2012).
[49] Z. Bai, Y. Su, SOAR: A Second-order Arnoldi Method for the Solution of the Quadratic Eigenvalue Problem, SIAM J. Matrix Anal. & Appl. 26 (3) (2005) 640–659. doi:10.1137/S0895479803438523.
[50] T.-J. Su, R. R. Craig, Model reduction and control of flexible structures using Krylov vectors, Journal of Guidance, Control, and Dynamics 14 (2) (1991) 260–267. doi:10.2514/3.20636.
[51] X. Wang, Y. Jiang, X. Kong, Laguerre functions approximation for model reduction of second order time-delay systems, J. Frankl. Inst. 353 (14) (2016) 3560–3577. doi:10.1016/j.jfranklin.2016.06.024.
[52] C. A. Beattie, S. Gugercin, Krylov-based model reduction of second-order systems with proportional damping, in: 2005 44th IEEE Conference on Decision and Control & European Control Conference, Institute of Electrical and Electronics Engineers, Piscataway, N.J, 2005, pp. 2278–2283. doi:10.1109/CDC.2005.1582501.
[53] P. Lietaert, K. Meerbergen, Comparing Loewner and Krylov based model order reduction for time delay systems, in: 2018 European Control Conference (ECC), IEEE, 2018, pp. 545–550. doi:10.23919/ECC.2018.8550614.
[54] Q. Aumann, E. Deckers, S. Jonckheere, W. Desmet, G. Müller, Code and data for numerical experiments in "Automatic model order reduction for systems with frequency-dependent material properties" (version 1.0) (Feb. 2022). doi:10.5281/zenodo.6225761.
[55] N. J. Higham, G. M. Negri Porzio, F. Tisseur, An Updated Set of Nonlinear Eigenvalue Problems.
URL http://eprints.maths.manchester.ac.uk/id/eprint/2699
[56] M. Sasso, G. Palmieri, D. Amodio, Application of fractional derivative models in linear viscoelastic problems, Mech. Time-Depend. Mat. 15 (4) (2011) 367–387. doi:10.1007/s11043-011-9153-x.
[57] E. Wegert, Visual Complex Functions, Birkhäuser, Basel, 2012. doi:10.1007/978-3-0348-0180-5.
[58] Y. Nakatsukasa, L. N. Trefethen, Reciprocal-log approximation and planar PDE solvers, SIAM Journal on Numerical Analysis 59 (6) (2021) 2801–2822. doi:10.1137/20m1369555.
[59] M. Stutz, M. Moser, M. Ochmann, Instability problems using the time domain BEM for impulse response calculations, in: The Sixth Forum Acusticum Aalborg, 2011, pp. 253–257.
[60] S. Jonckheere, E. Deckers, B. van Genechten, D. Vandepitte, W. Desmet, A direct hybrid Finite Element – Wave Based Method for the steady-state analysis of acoustic cavities with poro-elastic damping layers using the coupled Helmholtz–Biot equations, Comput. Methods Appl. Mech. Eng. 263 (2013) 144–157. doi:10.1016/j.cma.2013.04.013.
[61] Vigran, T. E., Kelders, L., Lauriks, W., Leclaire, P., Johansen, T. F., Prediction and Measurements of the Influence of Boundary Conditions in a Standing Wave Tube, Acta Acust. United Ac. 83 (3) (1997) 419–423.
[62] N. Atalla, M. A. Hamdi, R. Panneton, Enhanced weak integral formulation for the mixed (u,p) poroelastic equations, J. Acoust. Soc. Am. 109 (6) (2001) 3065–3068. doi:10.1121/1.1365423.

[63] A. Vermeil de Conchard, H. Mao, R. Rumpler, A perfectly matched layer formulation adapted for fast frequency sweeps of exterior acoustics finite element models, J. Comput. Phys. 398 (2019) 108878. doi:10.1016/j.jcp.2019.108878.

[64] M. Souza Lenzi, S. Lefteriu, H. Beriot, W. Desmet, A fast frequency sweep approach using Padé approximations for solving Helmholtz finite element models, J. Sound Vib. 332 (8) (2013) 1897–1917. doi:10.1016/j.jsv.2012.05.038.